



HAL
open science

Iodine local environment in high pressure borosilicate glasses: An X-ray photoelectron spectroscopy and X-ray absorption spectroscopy investigation

Yann Morizet, Valentin Jolivet, Nicolas Trcera, Tomo Suzuki-Muresan, Jonathan Hamon

► **To cite this version:**

Yann Morizet, Valentin Jolivet, Nicolas Trcera, Tomo Suzuki-Muresan, Jonathan Hamon. Iodine local environment in high pressure borosilicate glasses: An X-ray photoelectron spectroscopy and X-ray absorption spectroscopy investigation. *Journal of Nuclear Materials*, 2021, 553, pp.153050. <10.1016/j.jnucmat.2021.153050>. <hal-03238521>

HAL Id: hal-03238521

<https://hal.science/hal-03238521v1>

Submitted on 7 Oct 2021

HAL is a multi-disciplinary open access archive for the deposit and dissemination of scientific research documents, whether they are published or not. The documents may come from teaching and research institutions in France or abroad, or from public or private research centers.

L'archive ouverte pluridisciplinaire **HAL**, est destinée au dépôt et à la diffusion de documents scientifiques de niveau recherche, publiés ou non, émanant des établissements d'enseignement et de recherche français ou étrangers, des laboratoires publics ou privés.



HAL Authorization

1 **IODINE LOCAL ENVIRONMENT IN HIGH PRESSURE BOROSILICATE**
2 **GLASSES: AN X-RAY PHOTOELECTRON SPECTROSCOPY AND X-RAY**
3 **ABSORPTION SPECTROSCOPY INVESTIGATION**

4
5 **Yann MORIZET^{1,2*}, Valentin JOLIVET^{1,2,3}, Nicolas TRCERA⁴, Tomo SUZUKI-**
6 **MURESAN³, Jonathan HAMON¹**

7
8 ¹ Institut des Matériaux Jean Rouxel (IMN), Université de Nantes, UMR CNRS 6502, 2 rue
9 de la Houssinière, BP32229, 44322 Nantes Cedex 3, France

10
11 ² Université de Nantes, Nantes Atlantique Universités, Laboratoire de Planétologie et
12 Géodynamique de Nantes (LPGN), UMR CNRS 6112, 2 rue de la Houssinière, 44322 Nantes
13 Cedex, France

14
15 ³ SUBATECH (IMT Atlantique, CNRS/IN2P3, Université de Nantes), BP 20722, 44307
16 Nantes Cedex 3, France

17
18 ⁴ Synchrotron SOLEIL, L'Orme des Merisiers, Saint Aubin, BP 48, F-91192 Gif-sur-Yvette
19 Cedex, France

23 *Corresponding author: Yann Morizet

24 Postal address:

25 Laboratoire de Planétologie et Géodynamique (LPG), UMR-CNRS 6112, Université de

26 Nantes.

27 2 rue de la Houssinière, 44322 Nantes Cedex (FRANCE)

28 phone: +33 (0) 2 5112 5491

29 fax: +33 (0) 2 5112 5268

30 *E-mail: yann.morizet@univ-nantes.fr

31

32 **Keywords**

33 Nuclear waste glasses, Iodine dissolution mechanism, X-ray Absorption Spectroscopy, X-ray
34 Photoelectron Spectroscopy

35 **Abstract**

36 The ^{129}I radioactive isotope is a by-product of nuclear plants activity. Owing to its strong
37 volatility, there is currently no ideal protocol to immobilize ^{129}I in nuclear waste borosilicate
38 glasses. Recently, we have proposed the use of high-pressure syntheses to dissolve iodine in
39 various glass compositions; however, I speciation and dissolution mechanism could not be
40 determined.

41 We have adopted an approach combining X-ray Photoelectron Spectroscopy (XPS) and X-ray
42 Absorption Spectroscopy (XAS) methods to determine I speciation and molecular
43 environment in glasses containing from 0.5 to 2.5 mol.% I. The XPS spectra reveal that I is
44 mostly dissolved as iodide (>85% I^-) with a small proportion of elemental iodine (<15% I^0)
45 and the absence of iodate species (I^{5+}). For borosilicate glasses, the XAS results and
46 subsequent spectrum simulations suggested that Na and Ca are involved in the I^- vicinity with
47 averaged derived coordination number (CN) of 3.6 and 2.0 and bond length to the nearest
48 neighbour ($r_{\text{X-I}}$) 2.98 and 2.85 Å, respectively. These results suggest that the coexistence of
49 both I^- and I^{5+} species is not requested for electric neutrality but instead, we explain the I
50 speciation by the possible interplay with oxygen species from the borosilicate matrix. In
51 addition, the results imply that the borosilicate network is affected by the I dissolution.

52

53 **1. Introduction**

54 Among the many radioactive elements produced by anthropic nuclear activities, iodine (I) is
55 one important element representing a serious glitch in the effort for immobilizing radioactive
56 waste. One particular isotope (^{129}I) requires a special attention because of 1) its long half-life
57 (>15 Ma) and 2) its high mobility and volatility in environment. In particular, the high I
58 concentrations in surface water and atmosphere in industrial countries [1,2] is a health issue
59 considering that I can easily integrate the food chain and fix into living organisms [3,4].
60 Therefore, there is a need for a solution able to immobilize durably this isotope collected from
61 nuclear waste.

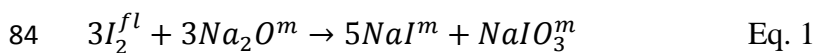
62 In a recent review, *Riley et al.* [5] provide an exhaustive view of the different methods used to
63 immobilize radioactive I in solid matrices. Either crystalline materials (e.g. [4,6-8]) or nuclear
64 waste glasses (e.g. [9-11]) could be used, however, it appears that there is currently no ideal
65 solution allowing the immobilization of radioactive I in a permanent and safe manner. For
66 instance, classical melting devices operating at ambient pressure do not allow the I retention
67 in significant concentrations in vitrified matrix [12]. At best, under ambient pressure
68 conditions a concentration <0.7 mol.% I can be retained in borosilicate glasses as shown in
69 previous works [9-11]. *Riley et al.* [10] reached almost 0.5 mol.% I in borosilicate glasses using
70 sealed ampoules (i.e. inside pressure above ambient pressure).

71 One potential solution to circumvent the strong I volatility during glass melting is to consider
72 the I conditioning in borosilicate glass matrix under extreme conditions: high-pressure.

73 Recent investigations [13-15] suggest that I solubility dramatically increases as the
74 confinement pressure increases. For instance, *Jolivet et al.* [15] reached I solubility up to 2.5
75 mol.% in nuclear waste glass compositions held at 1.5 GPa pressure. *Cicconi et al.* [14]
76 dissolved ~4 mol.% I in B_2O_3 -rich glass compositions held at pressure of 150 MPa; however,

77 their investigated compositions (~60 wt.% B₂O₃) were less relevant for the I immobilization
78 in nuclear waste matrices. A comparable behaviour was also observed as a function of
79 pressure for I in boron-free silicate glasses compositions with applications to Earth Sciences
80 [16,17]. *Leroy et al.* [17] showed that I solubility can reach up to 1.5 mol.% in Si-poor H₂O-
81 rich silicate glasses synthesised at 3.5 GPa.

82 One critical aspect is to clarify the I dissolution mechanism into the glass structure. Previous
83 works [10] proposed a generic equation for I dissolution in borosilicate glasses:



85 In this reaction, a diiodine molecule (I₂) from the fluid phase interacts with the Na⁺ cations to
86 form iodide (NaI) and iodate (NaIO₃) within the glass. In the proposed mechanism, Na is a
87 charge compensating cation to the BO₄ units within the structure [18-20]. Hence, removing
88 network modifying Na⁺ is likely to induce the interconversion of BO₄ to BO₃ units in order to
89 compensate the excess negative charges. However, the question remains debated, especially
90 as this mechanism is greatly function of the bulk chemical composition [18] and possibly
91 influenced by the intensive conditions for I-bearing glass synthesis. There is the coexistence
92 of different I oxidation states in Eq. 1: -1 in NaI and +5 in NaIO₃. In other words, the
93 structural analysis of I-bearing glass samples should reveal the presence of both I⁻ and I⁵⁺
94 species in order to satisfy the electrical charge neutrality.

95 Eq. 1 has been established based on XAS results [10] and to some extent, Raman
96 spectroscopic results [13]. The XAS (both X-ray Absorption Near-Edge Structure, XANES;
97 and Extended X-ray Absorption Fine Structure, EXAFS) is of particular interest as it probes
98 the local environment for a given element. It has been successfully applied for the
99 investigation of I local environment in various materials at both the K- and L-edges:
100 crystalline [4,21-23]; organic [24-26]; solution [27] and glass [9-11,14,28-30].

101 To the specific case of borosilicate glasses, the study of *McKeown et al.* [11] is a landmark
102 work. In a series of various borosilicate glasses typical of nuclear waste application, they
103 determined the local environment of dissolved I (up to 0.66 mol.%) using K-edge XAS
104 measurements at 33,169 eV. They applied the fingerprinting method (with crystalline
105 standards) to investigate the I K-edge XANES spectra and modelled the I K-edge EXAFS
106 spectra. Their results demonstrate that I dissolves in borosilicate glasses as I^- with a next
107 nearest neighbour at a distance of $\sim 3.04 \text{ \AA}$. They suggest that the next nearest charge
108 compensating cation is Na^+ and based on the EXAFS treatment that the coordination number
109 for I^- is ~ 4 . These results apply to borosilicate glasses synthesised at ambient pressure. The
110 effect of pressure is known to induce bond length and coordination changes (e.g. [31-34]);
111 therefore, the results obtained by *McKeown et al.* [11] may not apply to the case of borosilicate
112 glasses synthesised under high-pressure conditions.

113 In the present work, we have investigated the I local environment using L_3 -edge XAS (both
114 XANES and EXAFS). We have studied a series of borosilicate glasses synthesised under
115 high-pressure conditions (0.5-1.5 GPa) and reported in the work of *Jolivet et al.* [15]. In
116 addition, one sample having Na-free composition was also investigated for determining the
117 local environment around iodine atoms in the case of Ca surrounding. The range of I content
118 in the studied glasses is 0.5 to 2.5 mol.%. The I local environment was determined using
119 fingerprinting method for the XANES part and modelling of the EXAFS part using standard
120 crystalline structure. Based on these results and previous literature data, we propose a
121 discussion on the I dissolution mechanisms in borosilicate glasses synthesised under pressure
122 conditions.

123 **2. Analytical methods**

124 *2.1 Starting samples*

125 Several types of glass composition were used for this work. The samples as well as the
126 synthesis method are fully described in *Jolivet et al.* [15]. The investigated compositions are
127 two aluminoborosilicate glasses, International Simple Glass (ISG, [35]) and a Low Activity
128 Waste (LAW) glass called NH, and one boron-free aluminosilicate glass, TY. The
129 aluminoborosilicate glass compositions are in the system $\text{SiO}_2\text{-Al}_2\text{O}_3\text{-B}_2\text{O}_3\text{-CaO-Na}_2\text{O}$; the
130 ISG composition contains additional ZrO_2 (~1.7 mol.%). The TY aluminosilicate glass
131 composition is in the system $\text{SiO}_2\text{-Al}_2\text{O}_3\text{-CaO-Na}_2\text{O}$. Except for ISG (issued from an
132 industrial batch), the NH and TY compositions were prepared from a mixture of oxides (SiO_2 ,
133 B_2O_3 , Al_2O_3 , CaO) and sodium carbonate (Na_2CO_3). The powder mixtures were carefully
134 ground into an agate mortar and were melted twice in a Pt crucible at 1150°C for 1 h for NH
135 and at 1500°C for 20 h for TY (see [15] for details). Because the compositions studied by
136 *Jolivet et al.* [15] are both Na- and Ca-bearing glasses, discriminating the I local environment
137 between either Ca or Na is rendered difficult. Whereas the local charge compensation for I by
138 Na^+ cation is currently well admitted, the potential role for Ca^{2+} is currently not recognized.
139 Therefore, we also investigated one glass composition C35 that is a Na-free Ca-rich glass.
140 This investigated glass has the following composition: 31.8 SiO_2 , 29.2 B_2O_3 , 4.9 Al_2O_3 , 32.5
141 mol.% CaO ; as provided by the analyses from Scanning Electron Microscopy coupled with
142 Energy Dispersive X-ray Spectroscopy (SEM EDS).

143 We conducted the high-pressure experiments in a piston cylinder apparatus at temperatures
144 between 1300 and 1500°C and for pressures between 0.5 and 1.5 GPa using the pressurizing
145 protocol described in *Jolivet et al.* [15]. The volatile-free glass powder were mixed with a
146 known amount of solid I_2 . The mixture was loaded in a Pt capsule that was then sealed by arc-
147 welding. The run duration was ~4h and the sample was quenched to room temperature by
148 cutting off the power. The recovered samples consisted in clear glass covered with a dark
149 residue suggesting an I excess during the experiments. The I excess was removed by cleaning

150 in ethanol the glass samples. All the synthesised glasses was characterized by SEM EDS and
151 the I content ranges from 0.5 to 2.5 mol.% as reported in *Jolivet et al.* [15]. The I content
152 measured in C35 is 1.6 mol.%. The details of the sample composition are reported in *Jolivet et*
153 *al.* [15] and are given in *Supplementary Material* and the I content measured for each glass is
154 given in *Table 1*.

155 2.2 X-ray Photoelectron Spectroscopy

156 X-ray Photoelectron Spectroscopy was performed for several samples (see *Table 1*) to
157 determine the I speciation in our glasses with the aim to provide constraints for the EXAFS
158 simulations. Several crystalline standards (NaI, NaIO₃ and CaI₂O₆) were also analysed,
159 serving as a fingerprint for I speciation in the glasses. We could not acquire XPS spectra for
160 solid crystalline I₂ and CaI₂ owing to the sublimation of I₂ under high vacuum conditions and
161 the poor stability of CaI₂.

162 We carried out the XPS analyses with two spectrometers: a Kratos Nova and a Kratos Axis
163 Ultra using a monochromatic Al K α radiation operating at 1486.6 eV (15 kV, 20 mA) with a
164 charge neutralizer. The glass chips ($\sim 3 \times 3 \text{ mm}^2$) showing a surface fracture from the bulk of
165 the experimental charge were loaded into the sample chamber and at high vacuum ($< 10^{-8}$
166 mbar). The sample surface was not prepared and the analysis was conducted on a raw glass
167 surface, hence avoiding possible surface contamination. The spot size on the sample is
168 $300 \times 700 \text{ }\mu\text{m}^2$ area of analyses. We recorded survey spectra at a pass energy of 160 eV
169 corresponding to an overall instrument resolution measured on silver Fermi edge of 1.95 eV
170 and a step of 0.5 eV from -5 to 1200 eV. High resolution spectra of Na 1s, I 3d, O 1s, Ca 2p,
171 C 1s core levels were recorded with an instrument resolution measured on silver Fermi of
172 0.49 eV and a step of 0.1 eV at a pass energy of 20 eV. The calibrations were performed on
173 the adventitious C 1s in the binding energy at 284.8 eV [36,37]. All spectra were treated with

174 CasaXPS© software. All spectra were fitted with a U2 Tougaard function [38] for the
175 background and with a pseudo-Voigt function with a Lorentzian ratio of 50% for the various
176 peaks. Although, the associated error on the different components provided by the CasaXPS©
177 fitting package is relatively low owing to the good quality of the XPS spectra, we believe that
178 the simulations are accurate to within 10% of the derived value. Only the I 3d_{5/2} peak in the I
179 3d region with the highest intensity was fitted as compared to the one for the I 3d_{3/2}. The
180 obtained peak position did not show dependency on I content or glass composition. Therefore,
181 determining the exact nature of the charge-compensating cation (i.e. Na⁺ or Ca²⁺)
182 surroundings I atoms could not be possible. We obtained several acquisitions for each
183 element. We did not find any modification of each individual acquisition suggesting that the
184 glass is stable under the X-ray beam.

185 *2.3 X-ray Absorption Spectroscopy*

186 We collected the I L₃-edge XAS spectra on LUCIA beamline at SOLEIL synchrotron
187 operating with a current of 450/500 mA and an energy of 2.75 GeV [39]. The energy of the
188 incoming photons was selected by using double crystal monochromator Si(111). The XAS
189 spectra on the glass were collected in fluorescence mode with a silicon drift diode detector.
190 To avoid the self-absorption effect, the geometry of the beamline was set to a low angle
191 between the sample surface and the detector (2°). The energy calibration of the incoming
192 photons was achieved on titanium foil by selecting the first inflexion point of the spectrum at
193 4966 eV. We used in our experiment an unfocused beam with a size of 4x2 mm² for
194 maximizing the count rate. The glass powder samples were stuck on a copper plate using
195 carbon tape and acquisition were conducted under vacuum conditions. Prior to acquisition, the
196 region of interest for the X-ray fluorescence lines had to be optimised to avoid interferences
197 arising from the proximity between Ca K-edge fluorescence line (~3691 eV) and the I L₃-
198 edge fluorescence line (~3926 eV). The optimisation of the fluorescence region was

199 conducted such as that the higher tail of the Ca fluorescence line did not contribute to the I
200 signal. However, we suspect that removing the contribution of the Ca fluorescence line
201 appears to be incomplete, especially for C35 in which Ca is 20 times more concentrated than
202 I.

203 The XAS spectra were collected at the L₃-edge of I in the range 4510-4850 eV. For each
204 point, the counting time was 10 s. We collected at least three spectra on each sample in order
205 to obtain an average spectrum with a good signal to noise ratio. The recorded scans are
206 identical and the presented spectra correspond to an average of the different scans. A slight
207 colouring of the glass powder is observed after XAS acquisition. Several acquisitions were
208 also made on crystalline standards for comparison and fingerprinting of the XAS glass
209 spectra: NaI, CaI₂, I₂, NaIO₃, CaI₂O₆. In these crystalline compounds, the I oxidation state
210 varies from -1 in iodides to +5 in iodates. As a result, the XAS signal (XANES and EXAFS)
211 can be used for constraining the I oxidation state in the borosilicate glasses. Because
212 crystalline iodides (NaI and CaI₂) are highly sensitive to H₂O adsorption, the crystalline
213 sample powders were stored in a sealed glove box and quickly loaded into the vacuum
214 chamber for XAS analysis. We did not observe any visible sign of phase transformation under
215 X-ray beam; moreover, repetitive scans on the crystalline powders were almost identical.

216 Both XANES and EXAFS spectra were simulated to determine the I speciation in glasses and
217 the first coordination sphere around I atoms. The XAS spectra were reduced by using the
218 DEMETER package [40,41]. The normalisation and the merge of the XAS spectra as well as
219 the background removal were carried out with the Athena software [40,41]. In addition, the
220 self-absorption effect was checked using the Fluo software implemented in Athena [40,41].
221 The first coordination sphere to I atoms was obtained from the simulation of the EXAFS
222 signal by using the single scattering signals determined with known crystalline structure. We
223 used k²-weighted signal function in the k-space and the simulation of the EXAFS region was

224 done using the Artemis software [41]. A description of the EXAFS fitting protocol is provided
225 later in the Discussion section.

226 We simulated the ISG, NH, TY and C35 XANES spectra following the method described by
227 *Schlegel et al.* [25] using a linear combination of the crystalline compound spectra. Linear
228 fitting combinations were performed in the range 4540-4590 eV with the implemented tool in
229 Athena software. It should be emphasised that the choice of crystalline structure for EXAFS
230 or XANES spectrum simulations is based on the results obtained by the XPS, which provides
231 the I speciation in the investigated glasses.

232 **3. Results**

233 *3.1 Iodine speciation by XPS*

234 We determined the I oxidation state using the XPS technique. The XPS spectra for crystalline
235 compounds and glasses are shown in *Fig. 1*. We chose to represent only the 3d_{5/2} from the I
236 doublet peak for clarity and because it is the most intense peak compared to the 3d_{3/2} [42-44].
237 For crystalline powders, there is an obvious distinction in the XPS spectra between the I
238 oxidation states and therefore I local environment. For NaI in which I is present as -1
239 oxidation state, there is a peak located at ~619 eV; for NaIO₃ and CaI₂O₆ in which I is present
240 as +5 oxidation state, there is a peak located at ~624 eV. For I-bearing glasses studied here,
241 we observe in all the cases a single prominent peak located at ~619 eV (ranging from 619.0 to
242 619.4 eV obtained from the simulated spectra) and the absence of a peak at ~624 eV. The
243 presence of the peak at 619 eV suggests that I is dissolved in the glass mostly as I⁻ species. A
244 keener scrutiny reveals a peak at 624.4 eV for NH23-2 implying a small proportion of I⁵⁺
245 species within the glass. For several samples, we also observe a slight asymmetry on the high-
246 energy side of the 619 eV peak. We interpret this asymmetry as the possible presence of I₂
247 species [45]. This suggests the possible presence of I dissolved in glasses as I₂ species.

248 Furthermore, most of the investigated samples were clear glass indicating the absence of I₂-
249 filled bubbles. Brownish bubbles were only identified in TY glass samples and were
250 interpreted as bubbles filled with residual I₂.

251 Subsequent simulation of the I 3d_{5/2} peak reveals that I₂ is present as a dissolved species in
252 glass. In NH23-2 glass, we have identified the presence of I⁵⁺ at a total I fraction of 3.0%. The
253 results of the simulations are shown in [Table 1](#) with the I speciation and the XPS spectrum
254 simulations are provided in [Supplementary Material 1](#). In all investigated glasses, the
255 quantitative simulation of the peak reveals that I is present on average as 95.6% I⁻ and 4.1%
256 I₀, presumably I₂. The determination of the I speciation will be used for constraining the
257 simulations conducted on both the L₃-edge XANES and EXAFS.

258 Scrutinizing the I local environment with XPS simulations appears complicated, as the I 3d_{5/2}
259 peak position does not change as a function of glass composition. For instance, for C35 (i.e.
260 Na-free) for which the surrounding cation for I⁻ is Ca²⁺ exhibits a peak maximum at 619.2 eV
261 comparable to the peak position observed for the other glasses that are Na- and Ca-bearing
262 compositions.

263 *3.2 I L₃-edge XANES*

264 L₃-edge XANES spectra for crystalline and I-bearing glasses are shown in [Fig. 2](#). We provide
265 the entire set of spectra in [Supplementary Material 2](#). In [Fig. 2](#), all spectra exhibit a main
266 absorption edge located at ~4563 eV. There is no pre-edge peak observed. The crystalline I₂
267 spectrum is relatively featureless whereas the spectrum for other salts shows a distinguishable
268 edge peak at ~4563 eV, roughly symmetric except for NaI in which the edge peak seems to be
269 a composition of several components. For iodates (NaIO₃ and CaI₂O₆), there is a strong
270 shoulder with a maximum at ~4574 eV. This peak is not clearly visible for NaI, however, we
271 observe a peak at ~4570 eV and a broad feature extending up to ~4590 eV in the EXAFS

272 region. For the iodates, there is a strong broad asymmetric peak with a maximum at ~4592 eV
273 and corresponding to the beginning of the EXAFS region.

274 We followed the description provided by *Schlegel et al.* [25] for a tentative of assignment. The
275 peaks at ~4563 and ~4574 eV are attributed to the transition to 5d levels. The broad features
276 observed are assigned to 2p to d transitions [14]. We did not attempt to determine the I
277 oxidation state for crystalline compounds [46,47] as there is no apparent change in the edge
278 position, and also because the line broadening is important at the L edge for heavy elements
279 such as I. Instead, we use the crystalline spectra to decipher the I local environment in the
280 studied glasses.

281 The I L₃-edge XANES spectra are reported for six glass samples. It should be emphasised that
282 within a glass series (ISG, NH or TY) we did not observe any significant difference in
283 between the spectra (see *Supplementary Material 2*) suggesting that I has comparable local
284 environment for all samples of a given series. As observed in *Fig. 2*, the C35 XANES
285 spectrum contrast to the spectra for NH and ISG, therefore indicating that the I local
286 environment in C35 is not the same as the one in ISG and NH glasses. This observation
287 appears in contrast to the XPS results showing that I is dissolved as I⁻, regardless of the glass
288 composition. However, the XPS method only provides first level of information (i.e. I
289 oxidation state) and does not scrutinize the next nearest neighbour to the I atoms.

290 The XANES spectra for ISG and NH look alike to the spectrum of NaI and to a lower extent
291 to CaI₂. This suggests that ISG and NH spectra are possibly a combination of both NaI and
292 CaI₂ XANES spectra. There is a well-marked peak at ~4563 eV as well as a broad peak with a
293 maximum at ~4574 eV and a broad shoulder at ~4585 eV. Together, these features could
294 witness the presence of Ca- and/or Na-iodates or a mixture between iodates and Ca- and/or
295 Na-iodides; however, the XPS results obtained on those samples do not indicate the presence

296 of IO_3^- molecular species in the glass structure. We did not observe the presence of
297 unaccounted crystalline phase in the bulk of the glass as shown by the X-ray diagram obtained
298 [15]. Therefore, the XANES signal recorded corresponds to the I local environment in the
299 glass. The XANES spectrum for C35 that is Na-free glass composition has common features
300 with the XANES spectrum for CaI_2 , however, as observed in [Fig. 2](#), it appears unlikely that the
301 C35 spectrum will be reproduced with only the spectrum from CaI_2 . This observation
302 emphasises the difficulty to reproduce XANES spectrum for glasses with the sole use of
303 XANES spectrum from crystalline compounds.

304 Nonetheless, in [Fig. 3](#) we propose an attempt of XANES simulations using the method of
305 linear combination described by [Schlegel et al.](#) [25] to reproduce the XANES spectrum for the
306 glasses. We strongly emphasise that this approach represents only an attempt and is by no
307 mean an absolute result. The reason being that we simulate a XANES spectrum for a glass
308 using XANES spectra obtained on crystalline compounds: NaI , CaI_2 , I_2 , NaIO_3 and CaI_2O_6 ,
309 shown in [Fig. 2](#). The simulation results are also provided in [Table 1](#). The first step of the
310 simulation involved using the entire set of spectra for crystalline compounds without
311 constraints (except for C35 glass that is Na-free glass composition). We tested all the possible
312 combinations to obtain the fit using the Linear Fitting Combination package. The entire set of
313 simulation is provided in [Supplementary Material 2](#). The combination results involving
314 negative parameters were discarded. We limited the possible combination to three
315 independent components. From [Fig. 3](#), it can be observed that the simulated spectra do not
316 reproduce entirely the measured I-bearing glass spectra. As mentioned, it appears difficult to
317 completely reproduce the XANES glass spectra with the XANES crystalline spectra as it does
318 not take into consideration the variations in bond length or bond angle that is a specificity of
319 disordered glass materials (e.g. [48-52]).

320 The XANES spectrum for TY33 is reproduced with a combination of NaI (~66%), CaI₂
321 (~14%), and a non-negligible proportion of I₂ (~21%). Considering that TY33 contains 0.5
322 mol.% I, the proportion of I₂ ~0.1 mol.%. The presence of I₂ appears consistent with the fact
323 that TY glass samples showed a slight brownish colouring (see *Jolivet et al.* [15]). As shown in
324 [Table 1](#), the XANES simulation invoked the presence of iodate for several samples showing
325 the highest I content. Except for NH23-2, this result does not appear consistent with the XPS
326 results; however, at low concentration the presence of NaIO₃ would not be detected by XPS
327 measurements. For NH and ISG glasses, the XANES spectra are reproduced with a
328 combination of NaI and CaI₂ to more than 90% in proportion. The XANES simulations
329 suggest the presence of I₂ in ISG and TY glasses. The ISG33-2 appears to be a particular case
330 as the simulated amount of I₂ is relatively high (~40%); although this is not consistent with
331 the observed XPS results (see [Table 1](#)) suggesting that only 3.3% of I is dissolved as I₂. A
332 small contribution of iodate (CaI₂O₆) is suggested in all NH glasses. If we consider NH23-2
333 with 2.5 mol.% I dissolved, the proposed speciation will correspond to ~2.2 and ~0.3 mol.%
334 of iodide and iodate, respectively. For C35, the XANES spectrum is reproduced with a
335 contribution of 92.9 and 7.1% from CaI₂ and CaI₂O₆, respectively. This result is consistent to
336 a certain extent to the XPS result that suggests I to be dissolved as I⁻ species, although, the
337 presence of I⁵⁺ has not been identified.

338 From the general point of view the results illustrated in [Fig. 3](#) are consistent with the XPS
339 results given in [Table 1](#). The most important discrepancy is observed for ISG33-2 with ~40%
340 I₂ observed by XANES against 3% by XPS. In detail, it appears complicated to extract
341 reliable I species proportions from the simulation of the XANES spectrum owing to the
342 difficulty in simulating adequately the I L₃ XANES spectra for a glass with crystalline
343 compounds; therefore there is a large error associated to the derived proportion from XANES
344 simulation.

345 Although the associated error to the simulation is probably large and the spectra are not
346 reproduced adequately, it tends to discriminate the different iodide species present in the
347 glass. Invariably, the best linear combination induces the presence of NaI and CaI₂ suggesting
348 that both iodide species are present in the glasses. This aspect is also strengthened by the fact
349 that I can dissolve in the structure of the Na-free Ca-rich C35 glass composition. For instance,
350 we failed to simulate the spectra with one and not the other iodide crystalline spectrum.
351 Nonetheless, in the current work and the subsequent XANES simulations, we propose that
352 both Na⁺ and Ca²⁺ are involved into the charge compensation of the I⁻ species.

353 *3.3 I L₃-edge EXAFS*

354 I L₃-edge EXAFS spectra are shown in [Fig. 4](#) for several glasses. We classified the spectra as a
355 function of the I content and glass composition: from TY33 with 0.5 mol.% I to NH23-2 with
356 2.5 mol.% I. The spectrum for C35 is also added as this sample highlights the role of Ca²⁺
357 cations in the surrounding of I⁻ species. [Fig. 4A](#) represents the k²-weighted data. [Fig. 4B](#)
358 represents the amplitude of the radial distribution function (RDF) as obtained from the Fourier
359 transforms of the oscillatory k²-weighted EXAFS signal in the k-space. As a compromise
360 between short and long distance, we chose to use the k² oscillatory signal of the $\chi(k)$ function.
361 In the k-space, the signal to noise ratio (S/N) of the oscillatory signal is changing between
362 each sample. It appears that there is an increase in the S/N with increasing I content. For
363 instance, the NH23-2 with 2.5 mol.% I has a good S/N whereas TY33 with 0.5 mol.% the S/N
364 is relatively poor. Owing to the data quality and in order to keep for each sample analysis the
365 same range in the k-space spectra, the region used for the Fourier Transform of the EXAFS
366 spectra is set between 2.5 and 6.7 Å⁻¹. This limit at 6.7 Å⁻¹ corresponds to the higher point
367 usable for the data with the poor quality.

368 In [Fig.4B](#), the amplitude signal shows an intense peak with a maximum around 2.5 Å. This
369 peak corresponds to the I first neighbour atoms. Surprisingly, the peak maximum is at higher
370 position for C35: 2.82 Å, suggesting a longer distance to first neighbour. In addition, for C35
371 we observe a prominent peak located close to 1.5 Å that we explain by the possible existence
372 of I⁵⁺. This I⁵⁺ could be due to an evolution of the sample under the high energy of the X-ray
373 beam during XAS acquisition. It appears consistent with the suggested result of the XANES
374 fit but not with the XPS result that has a lower energy flux. In order to minimize the possible
375 artefacts in the signal for this peak in the fitting procedure, we applied a background filter in
376 the R space between 0 and 1.5 Å. The RDF peaks below 2.5 Å do not correspond to any
377 contribution from backscattering shells. In our case, the perturbations from the Ca excitation
378 in the glass (~500 eV below the I L₃-edge) can be considered weak compare to the noise due
379 to the amorphous structure of the glass that decreases the EXAFS signal quickly after the
380 threshold. The peak for TY33 is very weak and strongly overlapped with satellite scattering
381 signal. As inferred earlier, the low S/N in the k-space will affect the definition of the I nearest
382 neighbour in the R-space. Regardless of the glass chemical composition and I content, it
383 appears that the peak maximum, which does not correspond to the actual distance between I
384 atoms and its surrounding, are roughly identical to within <0.1 Å in radial distance. For
385 instance, in borosilicate glasses NH23-1 (1.9 mol.% I) has a peak maximum at 2.42 Å
386 whereas the ISG22-2 (1.2 mol.% I) has a peak maximum at 2.40 Å. The boron-free TY33 has
387 a peak maximum at 2.45 Å comparable to the one observed for borosilicate glasses NH and
388 ISG.

389 Hence, the distance between I and its surrounding for ISG, NH and TY would change
390 between 2.8 and 3.0 Å; and is possibly higher for C35. The estimated distance for ISG, NH
391 and TY is lower than the distance observed in iodide crystalline compounds: $r_{\text{Na-I}} = 3.24 \text{ \AA}$
392 [51] and $r_{\text{Ca-I}} = 3.12 \text{ \AA}$ [54]; however consistent with the distance reported in [McKeown et al.](#)

393 [11] of 3.04 Å in Na-bearing borosilicate glasses synthesised at ambient pressure. This
394 distance was attributed to I atoms surrounded by several Na atoms [10,11]. The estimated
395 distance to the nearest neighbour also seems consistent with the XANES simulation results
396 (*Fig. 3*) suggesting Ca and Na as the nearest neighbour to iodide species.

397 The objective in the treatment of the EXAFS spectra is to obtain an estimate on the
398 parameters for the first coordination sphere around I atoms: the average distance and the
399 coordination number to I atoms to the nearest neighbour. It should be emphasised that the
400 reported spectrum simulations and associated results represent only one possible solution. The
401 I EXAFS simulations were conducted in the radial distance range between ~1.5 and ~3.5 Å
402 (see *Fig. 5*). We could not investigate the signal to longer distance for several reasons: 1) the
403 EXAFS S/N ratio did not allow it as shown in *Fig. 4A* and 2) the proximity of the L₂-edge line
404 (~4850 eV) prevents from acquiring a long EXAFS signal. In order to obtain further
405 information about I second or third neighbours, we would require a longer k-space acquisition
406 than actually acquired. Due to the extremely low signal, we did not attempt to simulate the
407 EXAFS spectra for TY glass samples but only on ISG, NH and C35 glass spectra. To conduct
408 the simulations, we used standard crystalline structures taken from Crystallographic Open
409 Database ([55] and references therein): NaI and CaI₂. These structures were chosen in
410 agreement with the XPS results and XANES simulations that suggest the presence of mostly
411 iodide species dissolved in the glass structure. The presence of I₂ and CaI₂O₆ was not
412 considered in the simulation owing to the low abundances observed by XPS (see *Table 1*). For
413 the particular case of C35, we only used the scattering path from CaI₂ considering that the
414 glass composition is Na-free.

415 Prior to the simulation, the EXAFS spectra were calibrated for the scattering amplitude and
416 corrected for the edge position [56]. We simulated the spectrum obtained on CaI₂ with the
417 CaI₂ crystalline model. We obtained $S_0^2 = 0.984$ and $\Delta E_0 = -7.73$ eV. We took the single

418 scattering paths of each structure as given by the FEFF calculations in Artemis. For NaI, the
419 path Na to I has Coordination Number (CN_{Na-I}) = 6, r_{Na-I} = 3.236 Å; for CaI₂, CN_{Ca-I} = 3, r_{Ca-I}
420 = 3.117 Å. As [McKeown et al.](#) [11] derived an average CN_{Na-I} in their studied glasses close to
421 4, we choose a CN_{Na-I} = 4 and CN_{Ca-I} = 2 as starting guess prior to the simulations. The
422 simulations are conducted in several steps: 1) the optimization of the distance to the first
423 neighbour (r_{X-I}) is conducted with fixed initial coordination numbers (CN_{X-I}) and Debye-
424 Waller attenuation factor (σ^2); 2) the optimization of the σ^2 is conducted at fixed CN_{X-I} and r_{X-I} .
425 i; 3) the optimization of the CN_{X-I} is conducted at fixed σ^2 and r_{X-I} . Each category of
426 parameter (r , σ^2 or CN) is optimized for the whole set of scattering paths in the same time. We
427 repeated the procedure several times until obtaining the best possible fit of the radial distance
428 signal. We did not place any restraints on the parameter values to solve the EXAFS equation.

429 4. Discussion

430 4.1 Local environment of iodine in aluminoborosilicate glasses

431 EXAFS simulations are shown in [Fig. 5](#) for NH23-2, ISG22-2 and C35. We present for each
432 sample the fit of the RDF total amplitude ([Fig. 5A](#)) and the imaginary part ([Fig. 5B](#)). The fitting
433 results (CN_{X-I} , r_{X-I} and σ^2_{X-I}) are given in [Table 1](#) and [Supplementary Material 2](#).

434 The results obtained on the nearest neighbour distance to I are comparable to the previous
435 results from [McKeown et al.](#) [11]. For the iodide species (Ca-I and Na-I) and in the case of Na
436 and Ca-bearing glasses (NH, ISG and TY), we obtain distances changing from 2.76 to 3.01 Å.
437 On average the distance between I and Ca²⁺ is shorter than the distance to Na⁺, which can be
438 explained by the higher cationic charge of calcium for an equivalent ionic radius (1.20 and
439 1.24 Å for Na⁺ and Ca²⁺, respectively; [57]). We observe that the derived r_{X-I} are
440 systematically lower than the one reported in [McKeown et al.](#) [11] (i.e. 3.04 Å). One reason for
441 these lower I to first neighbour distances could be due to the intensive conditions (i.e. high-

442 pressure) at which our glasses were held considering that high-pressure conditions are known
443 to influence the local environment of cations [31-33]. On the other hand, as suggested, the
444 derived $r_{\text{Ca-I}}$ in the case of C35 is larger (3.60 Å) than the one derived for ISG and NH glasses.
445 This aspect is currently unexplained; however, it should be pointed out that the C35 glass
446 composition is significantly different from the ISG and NH glass compositions. It has more
447 B_2O_3 (~30 mol.%) and less SiO_2 (~30 mol.%) as compared to ISG and NH that could
448 therefore greatly influence the glass structure. Furthermore, it is currently well-accepted that
449 the distribution of network modifying cations within the glass structure is strongly affected by
450 the nature of those cations in the so-called mixed alkali or alkaline-earth effect [58-61]. In the
451 case of Na and Ca-mixed silicate glass compositions (for instance similar to ISG, NH and
452 TY), it has been shown that there is a strong intermixing between Ca^{2+} and Na^+ cations; in
453 other words the oxygen negative charge compensation is preferably accomplished by both
454 cations rather than only one sort of cation. As such, C35 represents a very peculiar glass
455 composition that cannot be readily compared to ISG and NH ones. Nevertheless, it has the
456 advantage to show that it is possible to find local environment of Γ^- species surrounded by
457 Ca^{2+} as a charge compensation cation.

458 We have reported the change in the derived $r_{\text{X-I}}$ as a function of I content in [Fig. 6A](#). The point
459 representative of C35 glass is not reported considering that this glass composition is not
460 similar to the NH and ISG ones. From [Fig. 6A](#), we do not observe a clear pattern as a function
461 of I content, however, it seems that the highest $r_{\text{X-I}}$ are observed for the highest I content. For
462 instance, in ISG glasses there is a slight increase in both Ca-I and Na-I bond lengths. We also
463 observe that the $r_{\text{X-I}}$ bond distances are systematically higher for NH glass than for ISG glass.
464 It suggests that the I local environment is probably a function of the glass bulk composition.
465 Typically, the difference observed in $r_{\text{Ca-I}}$ (>0.1 Å) might be explained by the change in Ca
466 content: 5.7 and 8.0 mol.% CaO in ISG and NH, respectively. This would also be consistent

467 with the higher $r_{\text{Ca-I}}$ (3.60 Å, see [Table 1](#)) observed for C35 having 32.5 mol.% CaO.
468 Although, $r_{\text{Na-I}}$ seems less affected (<0.1 Å) for a larger variation in Na₂O content: 12.6 and
469 24.2 mol.% Na₂O in ISG and NH, respectively. Considering the small number of investigated
470 compositions and samples, further work is currently requested to investigate the possible
471 change of $r_{\text{X-I}}$ as a function of both I content and glass bulk composition.

472 In a similar manner, we have plotted the change in the $\text{CN}_{\text{X-I}}$ values derived for iodide as a
473 function of I content in [Fig. 6B](#). The normalised $\text{CN}_{\text{X-I}}$ derived from the fit of the EXAFS
474 signal provided in [Table 1](#). For Ca, the CN changes from 1.5 to 2.2. For Na, the CN changes
475 from 2.3 to 4.2. The derived $\text{CN}_{\text{Na-I}}$ of 2.3 ± 0.2 is anomalously low and is obtained for ISG31
476 glass sample having a low I content (0.8 mol.%) and synthesised at the lowest pressure (0.5
477 GPa). As shown in [Fig. 6B](#), we do not observe any correlation between the derived CN and the
478 I content. The $\text{CN}_{\text{Ca-I}}$ exhibits the lowest variation in coordination number. The average $\text{CN}_{\text{Na-I}}$
479 and $\text{CN}_{\text{Ca-I}}$ (not including the C35 value of 1.5) are 3.6 ± 0.6 and 2.0 ± 0.1 , respectively. The
480 higher $\text{CN}_{\text{Na-I}}$ is consistent with the lower positive charges of Na as compared to Ca to
481 compensate the negative charges of the iodide.

482 The obtained CN values cover the lower end range reported in [McKeown et al.](#) [11] ([Fig. 7](#)). We
483 plotted the obtained normalised $\text{CN}_{\text{X-I}}$ values as a function of the obtained $r_{\text{X-I}}$ values for
484 iodide species in [Fig. 7](#). We also reported the experimental data points from [McKeown et al.](#)
485 [11] for comparison. We observe that our I-bearing glasses synthesised under high-pressure
486 conditions have comparable $r_{\text{X-I}}$ bond length as the one reported in [McKeown et al.](#) [11]. The
487 derived $\text{CN}_{\text{X-I}}$ have a narrower range as compared to the values reported in [McKeown et al.](#)
488 [11]. The possible reasons for lower $\text{CN}_{\text{X-I}}$ values could be: 1) the intensive pressure
489 conditions are responsible for the lower derived $\text{CN}_{\text{X-I}}$; 2) the higher dissolved I content
490 induces a lower global charge compensation in the surrounding of I⁻ species.

491 We applied bond valence theory using the bond valence parameters reported in *Brese and*
492 *O’Keeffe* [62]. We used the following equation that relates the I valence (v_{X-I}) to the bond
493 length (d_{X-I}):

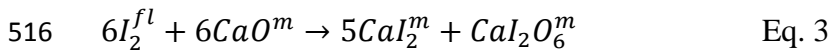
$$494 \quad v_{X-I} = \exp\left(\frac{R_{X-I} - d_{X-I}}{b}\right) \quad \text{Eq. 2}$$

495 Where X is the cation (i.e. Na^+ or Ca^{2+}), r_{X-I} is the bond valence parameter: 2.56 and 2.72 for
496 Na^+ and Ca^{2+} , respectively; b is a constant 0.37. The valence v_{X-I} is related to the CN with the
497 following relation $v = z/\text{CN}$, where z is the cation charge. Using the average CN derived from
498 EXAFS simulation (i.e. 3.6 and 2.0 for Na and Ca); we obtain d_{X-I} of 3.03 and 2.72 Å for Na-I
499 and Ca-I bond length, respectively. These values are in good agreement with the obtained
500 values in *Table 1* from EXAFS. The calculated d_{X-I} value for Ca-I bond appear lower than the
501 one derived from EXAFS (2.85 ± 0.09 Å on average for Ca-I). Bond valence theory calculates
502 a bond length without considering possible surrounding perturbation, however, Na^+ and Ca^{2+}
503 cations do not only share their positive charges to I^- anions but also to oxygen atoms from the
504 silicate and borate networks within the glass [63]. Thus, due to the perturbation brought by
505 surrounding oxygen atoms, the measured distance to I by EXAFS is expected to be different
506 from the one calculated with the bond valence theory.

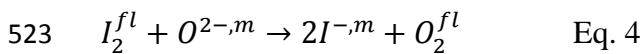
507 *4.2 Iodine dissolution mechanism during a high-pressure experiment under oxidizing* 508 *conditions*

509 In the present work, we have shown that I is mostly dissolved as iodide species (I^-). This
510 behaviour was expected and is consistent with previous studies on the I dissolution
511 mechanisms in borosilicate glasses [9-11,13] and the chemical reaction for I dissolution
512 represented by Eq. 1 in which an I_2 molecule from the fluid phase interacts with Na atoms in
513 the melt phase to form both NaI and NaIO_3 in the melt. Based on the XANES and EXAFS

514 results, we propose an additional reaction involving the Ca as a possible nearest neighbour for
515 I⁻ such as:



517 However, these two chemical reactions suffer from the fact that iodates are not observed in
518 our glasses or at extremely low concentrations; lower than the 1/5 ratio in Eq. 1 and 3. In the
519 absence of I⁵⁺ dissolved as iodate or the absence of cation capable of changing its oxidation
520 state (e.g. Fe changing from Fe²⁺ to Fe³⁺, [10]), there is an excess of negative charges due to
521 the reduction of I₂^{fl} into I⁻. One possible solution is to invoke an exchange between I and
522 oxygen from the melt with oxygen released in the fluid phase during the experiments such as:



524 Unfortunately, we have no way to test this hypothesis, besides we were not able to measure
525 the O₂^{fl} concentration at the capsule opening after the experiments. The nature of oxygen that
526 can be involved in this reaction is still to be determined [19,64-67]. At first level of
527 knowledge, the obvious candidate is to use Non-Bridging Oxygen (NBO) in the melt
528 structure, however, it could be NBOs from the silicate network or from the borate network
529 [19,65]. *Jolivet et al.* [15] suggested that the I dissolution is accompanied by a change in the
530 distribution of boron species (i.e. BO₃ and BO₄). Based on the Raman spectroscopic results,
531 they also showed that the silicate network appears unaffected by the I dissolution. In that case,
532 we expect an interplay between I atoms and the borate network with an increase in the BO₃
533 species and decrease in BO₄. If it is currently observed for ISG glass samples, it is the
534 opposite of NH glass samples: BO₄ increases with increasing I content and BO₃ decreases. In
535 any case, further experimental work is currently required using ¹⁷O NMR to determine the
536 nature of the oxygen involved in the dissolution mechanisms of iodine as I⁻ species.

537 **5. Conclusion**

538 In the subsequent work, we have investigated the local environment of I atoms dissolved in
539 glasses of various compositions synthesised under high-pressure conditions. To do so, we
540 used two complementary spectroscopic methods: XPS and I L₃-edge XAS. The studied
541 glasses are from three different compositions fully detailed in *Jolivet et al.* [15]. The range of I
542 investigated is 0.5 to 2.5 mol.%.

543 With the XPS, we show unambiguously that I is mostly dissolved as iodide (I⁻) species.
544 However, we could also observe small proportions of other species such I₂ and CaI₂O₆. Such a
545 speciation is also confirmed with the modelling of the I L₃-edge XANES using simple
546 spectrum linear combination. In addition, it also infers that Na⁺ is not the only nearest
547 neighbour of I atoms and we propose that Ca²⁺ cations are also acting as a charge balancing
548 cations to the negative charges on I⁻.

549 The simulation of the EXAFS spectra suggests that on average I⁻ anions has a bond length of
550 2.98 to 2.85 Å to the nearest neighbour, either Na⁺ or Ca²⁺. This range of values is consistent
551 with previous investigations. We derived a coordination number to Na of 3.6 and to Ca of 2.0.

552 The main outcome of those results is that Ca is able, like Na, to dissolve I in its surrounding.
553 This new observation is likely due to the high pressure conditions used for synthesising the I⁻
554 bearing borosilicate glasses. Although the question of I-bearing glass matrix is to be
555 determined, we show that solubilizing I in glass matrix at high pressure is a promising
556 protocol to immobilize radioactive ¹²⁹I in nuclear waste glasses.

557 *Acknowledgements*

558 The authors are grateful to the Région Pays de Loire that financed the current work through
559 the Pari Scientifique “CIPress” project. The authors thank the University of Nantes and the
560 CNRS for their access to analytical facilities. We acknowledge SOLEIL for provision of
561 synchrotron radiation facilities and we would like to thank LUCIA staff for assistance in

562 using the beamline. We wish to thank Prof. Nicolas Dacheux for handling our manuscript and
563 the three anonymous reviewers who helped for greatly improving our manuscript.

564 **References**

- 565 [1] Michel, R., Daraoui, E., Gorny, M., Jakob, D., Sachse, R., Tosch, L., Nies, H., Goroncy,
566 I., Herrmann, J., Synal, H.-A., Stocker, M., Alfimov, V., 2012. Iodine-129 and Iodine-127 in
567 European seawaters and in precipitation from Northern Germany. *Sci. Tot. Env.* 419, 151-
568 169.
- 569 [2] Chen, X., Gong, M., Yi, P., Aldahan, A., Yu, Z., Possnert, G., Chen, L., 2015. Distribution
570 of ^{129}I in terrestrial surface water environments. *Nuc. Inst. Meth. Phys. Res. B* 361, 604–608.
- 571 [3] Sinnott, B., Ron, E., Schneider, A.B., 2010. Exposing the thyroid to radiation: a review of
572 its current extent, risks, and implications. *Endocr. Rev.* 31, 756-773.
- 573 [4] Campayo, L., Grandjean, A., Coulon, A., Delorme, R., Vantelon, D., Laurencin, D., 2011.
574 Incorporation of iodates into hydroxyapatites: a new approach for the confinement of
575 radioactive iodine. *J. Mat. Chem.* 21, 17609.
- 576 [5] Riley, B.J., Vienna, J.D., Strachan, D.M., McCloy, J.S., Jerden, J.L.Jr., 2016. Materials
577 and processes for the effective capture and immobilization of radioiodine: A review. *J. Nuc.*
578 *Mat.* 470, 307-326.
- 579 [6] Watanabe, Y., Ikoma, T., Yamada, H., Suetsugu, Y., Komatsu, Y., Stevens, G.W.,
580 Moriyoshi, Y., Tanaka, J., 2009. Novel long-term immobilization method for radioactive
581 iodine-129 using a zeolite/apatite composite sintered body. *App. Mat. Interfaces* 1, 1579-
582 1584.
- 583 [7] Maddrell, E., Gandy, A., Stennett, M., 2014. The durability of iodide sodalite. *J. Nuc. Mat.*
584 449, 168–172.

585 [8] Coulon, A., Grandjean, A., Laurencin, D., Jollivet, P., Rossignol, S., Campayo, L., 2017.
586 Durability testing of an iodate-substituted hydroxyapatite designed for the conditioning of
587 ¹²⁹I. *J. Nuc. Mat.* 484, 324–331.

588 [9] Muller, I.S., McKeown, D.A., Pegg, I.L., 2014. Structural Behavior of Tc and I Ions in
589 Nuclear Waste Glass. *Proc. Mater. Sci.* 7, 53–59.

590 [10] Riley, B.J., Schweiger, M.J., Kim, D.S., Lukens, W.W., Williams, B.D., Iovin, C.,
591 Rodriguez, C.P., Overman, N.R., Bowden, M.E., Dixon, D.R., et al., 2014. Iodine solubility in
592 a low-activity waste borosilicate glass at 1000 °C. *J. Nuc. Mat.* 452, 178–188.

593 [11] McKeown, D.A., Muller, I.S., Pegg, I.L., 2015. Iodine valence and local environments in
594 borosilicate waste glasses using X-ray absorption spectroscopy. *J. Nuc. Mater.* 456, 182–191.

595 [12] Hmra, P., 2010. Retention of halogens in waste glass. U.S. department of energy.

596 [13] Cicconi, M.R., Pili, E., Grousset, L., Neuville, D.R., 2019a. The influence of glass
597 composition on iodine solubility. *Mat. Res. Soc.* 4, 17-18.

598 [14] Cicconi, M.R., Pili, E., Grousset, L., Florian, P., Bouillard, J.C., Vantelon, D., Neuville,
599 D.R., 2019b. Iodine solubility and speciation in glasses. *Sci. Rep.* 9, 7758.

600 [15] Jolivet, V., Morizet, Y., Paris, M., Suzuki-Muresan, T., 2020. High pressure
601 experimental study on iodine solution mechanisms in nuclear waste glasses. *J. Nuc. Mat.* 533,
602 152112.

603 [16] Bureau, H., Auzende, A.L., Marocchi, M., Raepsaet, C., Munsch, P., Testemale, D.,
604 Mézouar, M., Kubsky, S., Carrière, M., Ricolleau, A., et al., 2016. Modern and past volcanic
605 degassing of iodine. *Geochim. Cosmochim. Acta* 173, 114-125.

- 606 [17] Leroy, C., Bureau, H., Sanloup, C., Raepsaet, C., Glazirin, K., Munsch, P., Harmand, M.,
607 Prouteau, G., Khodja, H., 2019. Xenon and iodine behaviour in magmas. *Earth Planet.*
608 *Science Lett.* 522, 144–154.
- 609 [18] Dell, W.J., Bray, P.J., Xiao, S.Z., 1983. ^{11}B NMR studies and structural modeling of
610 $\text{Na}_2\text{O}-\text{B}_2\text{O}_3-\text{SiO}_2$ glasses of high soda content. *J. Non-Cryst. Solids* 58, 1–16.
- 611 [19] Du, L.S., Stebbins, J.F., 2005. Network connectivity in aluminoborosilicate glasses: A
612 high-resolution ^{11}B , ^{27}Al and ^{17}O NMR study. *J. Non-Cryst. Solids* 351, 3508-3520.
- 613 [20] Jolivet, V., Jossé, L., Rivoal, M., Paris, M., Morizet, Y., La, C., Suzuki-Muresan, T.,
614 2019. Quantification of boron in aluminoborosilicate glasses using Raman and ^{11}B NMR. *J.*
615 *Non-Cryst. Solids* 511, 50-61.
- 616 [21] Fuhrmann, M., Bajt, S., Schoonen, M.A.A., 1998. Sorption of iodine on minerals
617 investigated by X-ray absorption near edge structure (XANES) and ^{129}I tracer sorption
618 experiments. *App. Geochem.* 13, 127-141.
- 619 [22] Laurencin, D., Vantelon, D., Briois, V., Gervais, C., Coulon, A., Grandjean, A.,
620 Campayo, L., 2014. Investigation of the local environment of iodate in hydroxyapatite by
621 combination of X-ray absorption spectroscopy and DFT modelling. *RSC Adv.* 4, 14700-
622 14707.
- 623 [23] Podder, J., Lin, J., Sun, W., Botis, S.M., Tse, J., Chen, N., Hu, Y., Li, D., Seaman, J.,
624 Pan, Y., 2017. Iodate in calcite and vaterite: Insights from synchrotron X-ray absorption
625 spectroscopy and first-principles calculations. *Geochim. Cosmochim. Acta* 198, 218–228.
- 626 [24] Feiters, M.C., Küpper, F.C., Meyer-Klaucke, W., 2004. X-ray absorption spectroscopic
627 studies on model compounds for biological iodine and bromine. *J. Synchr. Rad.* 12, 85-93.

628 [25] Schlegel, M.L., Reiller, P., Mercier-Bion, F., Barré, N., Moulin, V., 2006. Molecular
629 environment of iodine in naturally iodinated humic substances: Insight from X-ray absorption
630 spectroscopy. *Geochim. Cosmochim. Acta* 70, 5536–5551.
631 *Inorg. Chem.* 4147–4152.

632 [26] Yamaguchi, N., Nakano, M., Tanida, H., Fujiwara, H., Kihou, N., 2006. Redox reaction
633 of iodine in paddy soil investigated by field observation and the I K-edge XANES
634 fingerprinting method. *J. Environ. Radioact.* 86, 212–226.

635 [27] Reed, W.A., May, I., Livens, F.R., Charnock, J.M., Jeapes, A.P., Gresley, M., Mitchell,
636 R.M., Knight, P., 2002. XANES fingerprinting of iodine species in solution and speciation of
637 iodine in spent solvent from nuclear fuel reprocessing. *J. Anal. At. Spectrom.* 17, 541–543.

638 [28] Rocca, F., Dalba, G., Fornasini, P., Tomasi, A., 1992. Structural study of AgI-Ag₂O-
639 B₂O₃ glasses by X-ray absorption spectroscopy. *Solid State Ionics* 53-56, 1253-1259.

640 [29] Lee, C.W., Pyo, J.-Y., Park, H.-S., Yang, J.H., Heo, J., 2017 Immobilization and bonding
641 scheme of radioactive iodine-129 in silver tellurite glass. *J. Nuc. Mat.* 492, 239-243.

642 [30] Chabauty, A.-L., Campayo, L., Méar, F.O., Montagne, L., 2019. Niobium- and bismuth-
643 silver phosphate glasses for the conditioning of radioactive iodine. *J. Non-Cryst. Solids* 510,
644 51-61.

645 [31] Allwardt, J.R., Stebbins, J.F., Terasaki, H., Du, L.-S., Frost, D.J., Withers, A.C.,
646 Hirschmann, M.M., Suzuki, A., Ohtani, E., 2007. Effect of structural transitions on properties
647 of high-pressure silicate melts: ²⁷Al NMR, glass densities, and melt viscosities. *Am. Mineral.*
648 92, 1093–1104.

649 [32] Lee, S.K., Kim, H.N., Lee, B.H., Kim, H.I., Kim, E.J., 2010. Nature of chemical and
650 topological disorder in borogermanate glasses: Insights from B-11 and O-17 Solid-State NMR
651 and quantum chemical calculations. *J. Phys. Chem. B.* 114, 412-420.

652 [33] Wilding, M., Guthrie, M., Kohara, S., Bull, C.L., Akola, J., Tucker, M.G., 2012. The
653 structure of MgO–SiO₂ glasses at elevated pressure. *J. Phys. Condens. Matter* 24, 225403–
654 225414.

655 [34] Morizet, Y., Vuilleumier, R., Paris, M., 2015. A NMR and molecular dynamics study of
656 CO₂-bearing basaltic melts and glasses. *Chem. Geol.* 418, 89–103.

657 [35] Gin, S., Abdelouas, A., Criscenti, L.J., Ebert, W.L., Ferrand, K., Geisler, T., Harrison,
658 M.T., Inagaki, Y., Mitsui, S., Mueller, K.T., et al., 2013. An international initiative on long-
659 term behavior of high-level nuclear waste glass. *Mater. Today* 16, 243–248.

660 [36] Barr, T.L., Seal, S., 1995. Nature of the use of adventitious carbon as a binding energy
661 standard. *J. Vac. Sci. Tech. A* 13, 1239-1246.

662 [37] Miller, D.J., Biesinger, M.C., McIntyre, N.S., 2002. Interactions of CO₂ and CO at
663 fractional atmosphere pressures with iron and iron oxide surfaces: one possible mechanism
664 for surface contamination? *Surf. Interface Anal.* 33, 299-305.

665 [38] Tougaard, S., 1997. Universality classes of inelastic electron scattering cross- sections.
666 *Surf. Inter. Anal.* 25, 137-154.

667 [39] Vantelon, D., Trcera, N., Roy, D., Moreno, T., Maily, D., Guillet, S., Metchalkov, E.,
668 Delmotte, F., Lassalle, B., Lagarde, P., Flank, A.M., 2016. The LUCIA beamline at SOLEIL.
669 *J. Synchr. Rad.* 23, 635-640.

670 [40] Newville, M., Ravel, B., Haskel, D., Rehr, J. J., Stern, E.A., Yacoby, Y., 1995. Analysis
671 of multiple-scattering XAFS data using theoretical standards. *Physica B* 208/209, 154–156.

672 [41] Ravel, B., Newville, M., 2005. ATHENA, ARTEMIS, HEPHAESTUS: data analysis
673 for Xray absorption spectroscopy using IFEFFIT. *J. Synchr. Rad.* 12, 537–541.

674 [42] Tojo, T., Tachikawa, T., Fujitsuka, M., Majima, T., 2008. Iodine-doped TiO₂
675 photocatalysts: Correlation between band structure and mechanism. *J. Phys. Chem. C* 112,
676 14948–14954.

677 [43] Marinoiu, A., Gatto, I., Raceanu, M., Varlam, M., Moise, C., Pantazi, A., Jianu, C.,
678 Stefanescu, I., Enachescu, M., 2017. Low cost iodine doped graphene for fuel cell electrodes.
679 *Int. J. Hydrogen Energy* 42, 26877-26888.

680 [44] Xiang, P., Lv, F., Xiao, T., Jiang, L., Tan, X., Shu, T., 2018. Improved performance of
681 quasi-solid-state dye-sensitized solar cells based on iodine-doped TiO₂ spheres photoanodes.
682 *J. Alloys Compounds* 741, 1142-1147.

683 [45] Moulder, J.F., Stickle, W.F., Sobol, P.E., Bomben, K.D., 1992. Handbook of W-ray
684 Photoelectron Spectroscopy: a reference book of standard spectra for identification and
685 interpretation of XPS spectra. J. Chastain Ed., Perkin-Elmer Corporation Physical Electronics
686 Division, Eden Prairie, Minnesota.

687 [46] Brown, G.E.Jr., Calas, G., Waychunas, G.A., Petiau, J., 1988. X-ray absorption
688 spectroscopy and its applications in mineralogy and geochemistry. *Rev. Mineral.* 18, 431-512.

689 [47] Henderson, G.S.F., de Groot, M.F., Moulton, B.J.A., 2014. X-ray Absorption Near-Edge
690 Structure (XANES) spectroscopy. *Rev. Min. Geochem.* 78 pp. 75-138.

691 [48] Du, J., Cormack, A.N., 2004. The medium range structure of sodium silicate glasses: a
692 molecular dynamics simulation. *J. Non-Cryst. Solids* 349, 66-79.

693 [49] Benoit, M., Profeta, M., Mauri, F., Pickard, C.J., Tuckerman, M.E., 2005. First-principles
694 calculation of the ^{17}O NMR parameters of a calcium aluminosilicate glass. *J. Phys. Chem. B*
695 109, 6052-6060.

696 [50] Farnan, I., Grandinetti, P.J., Baltisberger, J.H., Stebbins, J.F., Werner, U., Eastman,
697 M.A., Pines, A., 1992. Quantification of the disorder in network-modified silicate glasses.
698 *Nature* 358, 31-35.

699 [51] Liu, Y., Nekvasil, H., Tossell, J., 2005. Explaining the effects of T-O-T bond angles on
700 NMR chemical shifts in aluminosilicates: A Natural Bonding Orbital (NBO) and Natural
701 Chemical Shielding (NCS) analysis. *J. Phys. Chem. A* 109, 3060-3066.

702 [52] Massiot, D., Messinger, R.J., Cadars, S., Deschamps, M., Montouillout, V., Pellerin, N.,
703 Veron, E., Allix, M., Florian, P., Fayon, F., 2013. Topological, geometric, and chemical order
704 in materials: insights from solid-state NMR. *Acc. Chem. Res.* 46, 1975–1984.

705 [53] Wyckoff, R.W.G., 1963. *Rocksalt structure Crystal Structures*, Second edition.
706 Interscience Publishers, New York, New York, 1963, 1, 85-237.

707 [54] Blum, H., 1933. Die Kristallstruktur des wasserfreien Magnesiumjodids und
708 Calciumjodids. *Zeitschrift fuer Physikalische Chemie, Abteilung B: Chemie der*
709 *Elementarprozesse, Aufbau der Materie* 22, 298-304.

710 [55] Quirós, M., Gražulis, S., Girdzijauskaitė, S., Merkys, A., Vaitkus, A., 2018. Using
711 SMILES strings for the description of chemical connectivity in the Crystallography Open
712 Database. *J. Cheminformatics* 10, 23.

713 [56] Morizet, Y., Trcera, N., Larre, C., Rivoal, M., Le Menn, E., Vantelon, D., Gaillard, F.,
714 2019. X-ray absorption spectroscopic investigation of the Ca and Mg environments in CO_2 -
715 bearing silicate glasses. *Chem. Geol.* 510, 91–102.

716 [57] Whittaker, E.J.W., Muntus, R., 1970. Ionic radii for use in geochemistry. *Geochim.*
717 *Cosmochim. Acta* 34, 945-956.

718 [58] Lee, S.K., Stebbins, J.F., 2003. Nature of cation mixing and ordering in Na-Ca silicate
719 glasses and melts. *J. Phys. Chem. B* 107, 3141-3148.

720 [59] Allwardt, J.R., Stebbins, J.F., 2004. Ca-Mg and K-Mg mixing around non-bridging O
721 atoms in silicate glasses: An investigation using ^{17}O MAS and 3QMAS NMR. *Am. Mineral.*
722 89, 777-784.

723 [60] Kelsey, K.E., Allwardt, J.R., Stebbins, J.F., 2008. Ca-Mg mixing in aluminosilicate
724 glasses: An investigation using ^{17}O MAS and 3QMAS and ^{27}Al MAS NMR. *J. Non-Cryst.*
725 *Solids* 354, 4644-4653.

726 [61] Le Losq, C., Neuville, D.R., 2013. Effect of the Na/K mixing on the structure and the
727 rheology of tectosilicate silica-rich melts. *Chem. Geol.* 346, 57-71.

728 [62] Brese, N.E., O'Keeffe, M., 1991. Bond-valence parameters for solids. *Acta Crystallogr. B*
729 47, 192-197.

730 [63] Cormier, L., Cuello, G.J., 2013. Structural investigation of glasses along the MgSiO_3 -
731 CaSiO_3 join: Diffraction studies. *Geochim. Cosmochim. Acta* 122, 498-510.

732 [64] Stebbins, J.F., Zhao, P., Kroeker, S., 2000. Non-bridging oxygens in borate glasses:
733 characterization by ^{11}B and ^{17}O MAS and 3QMAS NMR. *Solid State Nuc. Magn. Res.* 16, 9-
734 19.

735 [65] Du, L.S., Allwardt, J.R., Schmidt, B.C., Stebbins, J.F., 2004. Pressure-induced structural
736 changes in a borosilicate glass-forming liquid: Boron coordination, non-bridging oxygens,
737 and network ordering. *J. Non-Cryst. Solids* 337, 196-200.

738 [66] Lee, S.K., Sung, S., 2008. The effect of network-modifying cations on the structure and
739 disorder in peralkaline Ca-Na aluminosilicate glasses: O-17 3Q MAS NMR study. Chem.
740 Geol. 2008, 256, 326-333.

741 [67] Morizet, Y., Florian, P., Paris, M., Gaillard, F., 2017. ¹⁷O NMR evidence of free ionic
742 clusters Mⁿ⁺ CO₃²⁻ in silicate glasses: Precursors for carbonate-silicate liquids immiscibility.
743 Am. Mineral. 102, 1561–1564.

744

745 **Figure caption**

746 Figure 1: XPS spectra in the I 3d_{5/2} energy region obtained on I-bearing glasses of ISG and
747 NH compositions from *Jolivet et al.* [15] along with XPS spectra for crystalline compounds:
748 NaI, NaIO₃ and CaI₂O₆. The peak at ~619 eV is attributed to I⁻ species and the peak at ~624
749 eV is attributed to I⁵⁺ species.

750 Figure 2: I L₃-edge XANES spectra for I-bearing glasses (ISG, NH, TY and C35) and solid
751 crystalline compounds (I₂, NaI, CaI₂, NaIO₃ and CaI₂O₆) in the 4540-4600 eV region. The
752 strong feature at 4563 eV corresponds to the white line and is visible on almost all spectra
753 except I₂ that exhibits relatively featureless spectrum. There are two broad peaks located at
754 ~4574 and 4590 eV are assigned to transitions in the 5d levels and 2p to d, respectively.

755 Figure 3: Linear Combination Fitting of the I L₃-edge XANES spectra for I-bearing glasses
756 (A, TY33; B, ISG22-2; C, NH23-2; and D, C35) with spectra from crystalline compounds.
757 The residual from the fit is also shown. The derived proportion of each component is reported
758 and is a combination of NaI, CaI₂, I₂ and to a lower part CaI₂O₆ (see *Table 1*).

759 Figure 4: Typical I L₃-edge EXAFS spectra for investigated glasses and represented in the k-
760 space (A) and R-space (B). Spectra are stacked with increasing I content from TY33 (0.5
761 mol.%) to NH23-2 (2.5 mol.%). In addition, spectrum from C35 (1.6 mol.%) is also reported.
762 The strong peak at ~2.5 Å corresponds to the actual EXAFS signal for the nearest neighbour
763 of the I atoms.

764 Figure 5: Examples of I L₃-edge EXAFS simulation of the RDF for NH23-2 (A), ISG22-2 (B)
765 and C35 (C). The simulation of the imaginary part of the EXAFS signal is also shown. The
766 simulation are conducted in the 1.5 to 3.5 Å region to derive the CN_{X-I} and r_{X-I}. We used
767 single scattering paths from crystalline structure: NaI and CaI₂, in agreement with the

768 observed components from XANES simulations. The EXAFS fitting results are reported in
769 [Table 1](#).

770 Figure 6: Change in the derived r_{X-I} in Å (A) and CN_{X-I} (B) from EXAFS simulations as a
771 function of I content in mol.%. The data are reported for Ca-I and Na-I and for ISG and NH
772 glass compositions. The error bars on each point is determined from the EXAFS fitting
773 results.

774 Figure 7: Change in the I CN as a function of r_{X-I} in Å. Data are obtained from EXAFS
775 simulations of the I-bearing studied glasses (ISG and NH) and are compared to the data
776 obtained by [McKeown et al.](#) [11]. The values for crystalline compounds are also shown.